Solution-processed graphene–nanographene van der Waals heterostructures for photodetectors with efficient and ultralong charge separation

Zhaoyang Liu, Haixin Qiu, Shuai Fu, Can Wang, Xuelin Yao, Alex Dixon, Stéphane Campidelli, Egon Pavlica, Gvido Bratina, Shen Zhao, et al.

Solution Processed Graphene-Nanographene van der Waals Heterostructures for Photodetectors with Efficient and Ultralong Charge Separation

Zhaoyang Liu,[†,⊥] Haixin Qiu,[†,⊥] Shuai Fu,[‡,⊥] Can Wang,[†] Xuelin Yao,[‡] Alex G. Dixon,[§] Stéphane Campidelli,[▽] Egon Pavlica,[§] Gvido Bratina,[§] Shen Zhao,[#] Loïc Rondin,[#] Jean-Sébastien Lauret,[#] Akimitsu Narita,[‡,∥] Mischa Bonn,[‡] Klaus Müllen,[‡] Artur Ciesielski,[†] Hai I. Wang,[*,‡] Paolo Samorì[*,†]

[†] University of Strasbourg, CNRS, ISIS UMR 7006, 8 allée Gaspard Monge, 67000 Strasbourg, France

[‡] Max Planck Institute for Polymer Research, Ackermannweg 10, 55128 Mainz, Germany

[§] Laboratory of Organic Matter Physics, University of Nova Gorica, Vipavska 13 Nova, Gorica SI-5000, Slovenia

[▽] Université Paris-Saclay, CEA, CNRS, NIMBE, LICSEN, 91191, Gif-sur-Yvette, France

[#] Université Paris-Saclay, ENS Paris-Saclay, Centrale Supélec, CNRS, LuMIn, 91190, Orsay, France

[∥] Organic and Carbon Nanomaterials Unit, Okinawa Institute of Science and Technology Graduate University, 1919-1 Tancha, Onna-son, Kunigami, Okinawa 904-0495, Japan

Keywords: graphene, nanographene, van der Waals heterostructures, ultralong charge separation

ABSTRACT: Sensitization of graphene with inorganic semiconducting nanostructures has been demonstrated as a powerful strategy to boost its optoelectronic performance. However, the limited tunability of optical properties and toxicity of metal cations in the inorganic sensitizers prohibits their widespread applications, and the in-depth understanding of the essential interfacial charge transfer process within such hybrid systems remains elusive. Here, we design and develop high-quality nanographene (NG) dispersions with a large-scale production using high-shear mixing exfoliation. The physisorption of these NG molecules onto graphene gives rise to the formation of graphene-NG van der Waals heterostructures (VDWHs), characterized by strong interlayer coupling through π-π interactions. As a proof of concept, photodetectors fabricated based on such VDWHs show ultrahigh responsivity up to 4.5×10^7 A/W and a specific detectivity reaching 4.6×10^{13} Jones, being competitive with the highest values obtained for graphene-based photodetectors. The outstanding device characteristics is attributed to the efficient transfer of photogenerated holes from NGs to graphene and the long-lived charge separation at graphene-NG interfaces (beyond 1 ns), as elucidated by ultrafast terahertz (THz) spectroscopy. These results demonstrate the great potential of such graphene-NG VDWHs as prototypical building blocks for high-performance, low toxicity optoelectronics.

Introduction

Graphene is highly attractive in photonics and optoelectronics applications thanks to its extraordinary physical properties.[1-8] However, the modest light absorption of monolayer graphene[7-9] and the short (~picosecond) lifetime of the photo-generated hot carriers[9-11] result in relatively low internal quantum efficiency,[8] thus limiting the availability of pristine graphene in photodetection.[6-8, 12-14]

Hybrid systems based on a viable sensitization approach with inorganic semiconducting nanostructures have been demonstrated to boost the graphene-based device performance significantly.[15-20] Unfortunately, toxic heavy metals limit their real-life applications due to their severe impact on human health and the environment.[21] Moreover, the size-dependent band structures and the lack of *ad hoc* optical properties of the inorganic sensitizers hinder their potential for broadband and tunable photodetection in the ultraviolet (UV) and infrared (IR) ranges.[22] Graphene-MoS_2 van der Waals heterostructures (VDWHs) have been demonstrated and shown remarkable optoelectronic functionality.[23-24] Nevertheless, the lack of control over the lattice alignment at the interface between the 2D nanosheets, and the strong layer-dependent band structures of MoS_2, as well as the significant complexity of the device fabrication with multi-step transfer process, determines such conventional 2D-2D VDWHs cannot meet the ultimate requirements for programming highly ordered superlattices to efficiently improve the optoelectronic performance of graphene.

In this context, the use of organic compounds as solution processed sensitizers can be appealing for graphene-based optoelectronic devices, thanks to their ease of synthesis, size- and structure-tunable optoelectronic properties. One major challenge for using organic sensitizers lies in the considerable exciton binding energy originating from the reduced charge screening effects, which limit the charge transport in the photoactive materials and charge separation at interfaces and thus reduces the overall device performance.[25-26] Thus, developing ultrafast transport channels by e.g., enhancing the sensitizer-graphene interfacial electronic coupling to boost the charge transfer efficiency is highly desirable. In this regard, the construction of VDWHs using graphene and its structurally similar components may lead to new fascinating opportunities to increase the interlayer coupling for efficient optoelectronics.

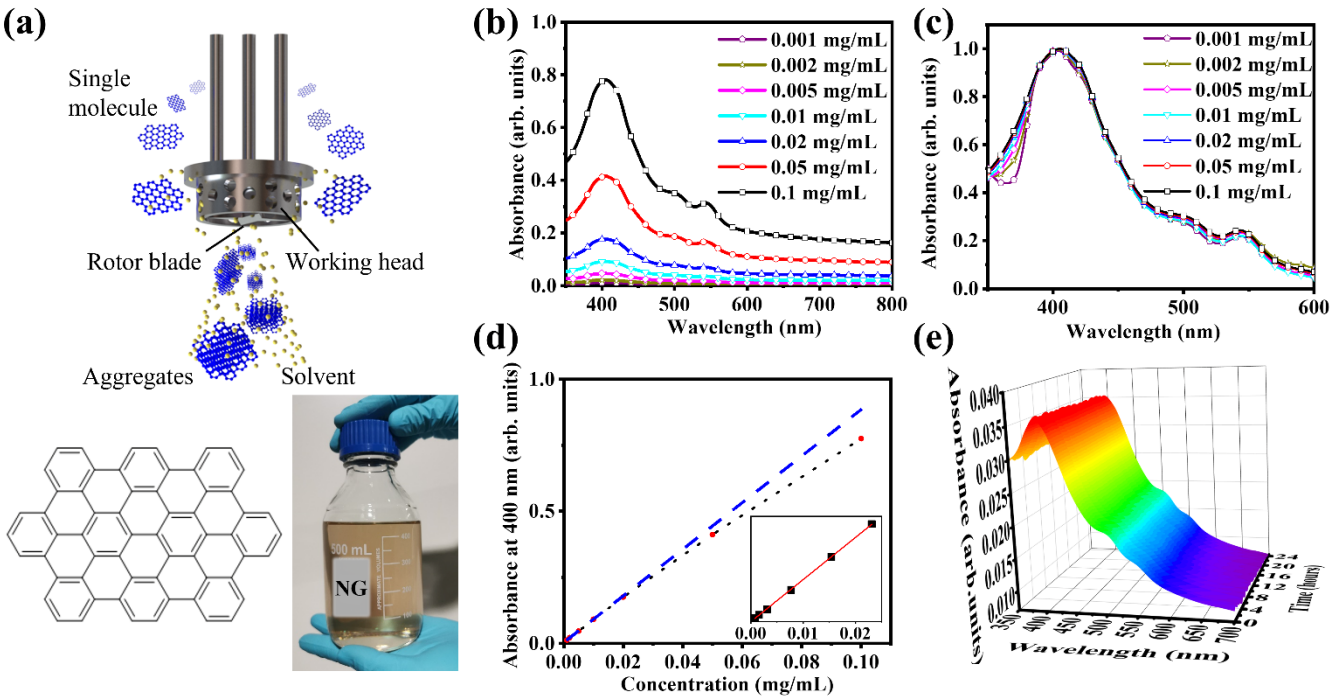

Figure 1. Shear mixing exfoliation of the NG aggregates. **a)** Schematic illustration of the shear mixing exfoliation process to achieve monodispersed NG molecules. Molecular structure of the employed NG, i.e., $C_{60}H_{22}$. Picture of 0.5 Liter NG dispersion at 0.004 mg mL^{-1} concentration in NMP, suggesting the potential for scale-up production. **b)** UV-Vis absorption spectrum of the obtained NG dispersion in NMP with different concentrations, from 0.001 to 0.1 mg mL^{-1}. **c)** Normalized UV-Vis absorption of NG dispersion with different concentrations, from 0.001 to 0.1 mg mL^{-1}. **d)** Absorbance at 400 nm as a function of NG concentration. Inset shows a good linear fitting with R^2=0.9997 at lower concentrations. **e)** Stability test of NG dispersion: UV-Vis absorption spectrum during 24 hours.

The bottom-up synthesized nanographene (NG) molecules, with their discotic nanoscale 2D structures, are promising candidates as sensitizers in graphene-based VDWHs due to their close structural similarity with graphene lattices and programmable electronic and optical properties. These two characteristics could facilitate the self-assembling behavior and allow for efficient interfacial charge transfer through strong π-π interactions with matching lattices.[27] However, extended aromatic structures with strong intermolecular π-π interactions typically lead to insoluble NG aggregates, which is detrimental to their optical properties. Ideally, the NG molecules should be easily processable in common organic solvents and form a self-assembled, monolayer-thick molecular layer on graphene. Although the solubility issue has been partially solved by introducing aliphatic side chains, it is still challenging to suppress the detrimental intermolecular interactions for large NGs, thus drastically lowering the optoelectronic quality of the molecule and assemblies thereof.[28-31] Thus, it is highly appealing to overcome the strong intermolecular π-π interactions within NG aggregates by isolating the molecules in the liquid phase and enabling their processing as monomolecular absorbate layers onto microscale high-quality graphene flakes, thereby realizing strongly coupled graphene-NG VDWHs for optoelectronics.

Herein, we employed high-shear mixing to break the aggregates of stacked NG molecules. The obtained NG dispersions follow the Beer-Lambert behavior across a concentration range from 0.001 to 0.02 mg mL^{-1}, demonstrating the high homogeneity, and thus the efficient exfoliation of the NG aggregates. The STM studies of ultrathin films of unsubstituted NG physisorbed onto graphite substrate revealed the existence of NGs in monodisperse form. Furthermore, the NG dispersion is drop-casted onto mechanically exfoliated graphene flakes to form graphene-NG VDWHs, where the NG molecules act as the nanoscale light-absorbers and graphene acts as the electron transport layer. As a proof of concept, photodetectors based on such graphene-NG VDWHs display an ultrahigh responsivity of 4.5×10^7 A/W and a specific detectivity of 4.6×10^{13} Jones, being competitive with the highest values obtained for graphene-based photodetectors. By employing THz spectroscopy, we attribute the excellent device characteristics to an ultralong charge separation (beyond 1 ns) at graphene-NG interfaces following the ultrafast, highly efficient transfer of holes from NGs to graphene. This work demonstrates the great potential of such graphene-NG VDWHs as prototypical active components for high-performance optoelectronics without toxic materials.

Results and discussion

Recently, it has been demonstrated that high-shear mixing can weaken and eventually break the van de Waals interactions between the 2D sheets of graphite, enabling the production of defect-free graphene in large quantities.[32] Here, we extend this approach to disrupt the aggregates of large and unsubstituted NGs, which are powder form materials after organic synthesis. **Figure 1**a shows the molecular structure of the employed NG molecule, which is the most thermodynamically stable isomer of $C_{60}H_{22}$, synthesized as previously reported.[33] A scheme of the proposed high-shear mixing exfoliation process of NG is also depicted in Figure 1a, where the high-speed rotation of the rotor blades generates a powerful suction pulling the aggregates at

the bottom into the working head. The intense hydraulic shear will then extrude out the NG and the solvent molecules together from the periphery of the working head. *N*-methyl-2-pyrrolidone (NMP), a commonly used solvent for graphene and carbon nanotube exfoliation, is chosen as the operating solvent because its surface energy matches well with the graphene lattice.[32, 34] Under a 4000 rpm rotor speed for only 30 mins, the NG can be readily exfoliated into homogeneous dispersions. The production of 1 L/h of NG dispersion within our current lab capacity provides unambiguous evidence for the huge potential of the shear mixing exfoliation for the large-scale production of NGs, which can be readily upscaled to tens of L/h in an industrial production line. The resulting NG dispersion is stable for at least one week without significant precipitation, thanks to the matched surface energies between the basal plane of NG (same as graphene) and the NMP solvent. Since the absorbance of NG molecules is highly sensitive to their aggregation states, UV-Vis absorption is employed to gain quantitative insight into the extent of aggregation.[31] The shear mixing approach results in sharp absorption features with the first dominant absorption centered around 400 nm, indicating an extremely limited aggregation and consequently very narrow thickness distributions for exfoliated NGs. In stark contrast, NG dispersions obtained by other approaches, e.g., *via* prolonged ultrasonication (500W, for 3 hours), show much broader absorption peaks (Figure S1). This indicates the existence of various types of aggregates within the dispersion and the low production yield of the conventional sonication approach. Therefore, the shear-mixing approach is far more advantageous over the conventional ultrasonication method in terms of both scalability and quality of achieved dispersion. Figure 1b shows the UV-Vis absorption spectra of exfoliated NG dispersions in NMP at different concentrations, ranging from 0.001 to 0.1 mg mL^{-1}, which are all dominated by an optical transition of excitonic origin featuring at ~400 nm, and are highly consistent with NG of the same aromatic core structure but bearing alkyl chains.[33] By normalizing all the absorption curves as shown in Figure 1c, the ratio between the absorbance at 365 nm and 400 nm (Abs_{365nm}/Abs_{400nm}) is shown to gradually increase from 43% to 60% with increasing NG concentration from 0.001 to 0.1 mg/mL, showing sharper feature of the absorption curve at lower concentrations.[31] Such a phenomenon suggests a decreased amount of aggregated NGs in diluted conditions, thereby offering useful hints for the optimization of the shear mixing process as well as the subsequent self-assembly-driven film formation. The absorbance values at 400 nm and 500 nm, plotted as a function of the concentration, comply very well with the Beer-Lambert behavior from 0.001 to 0.02 mg mL^{-1}, demonstrating the high homogeneity of the obtained dispersion and thus good exfoliation of the NG aggregates, as displayed in Figure 1d and Figure S2. The monomer fraction begins to drop from 91% to 86%, with the concentration increasing from 0.05 to 0.1 mg mL^{-1}, showing certain aggregations at higher concentrations. Figure 1e reveals the absence of significant changes in absorption spectra during 24 hours, demonstrating the superior stability of the high-shear mixing obtained NG dispersion.

To further verify the quality of the exfoliated NG molecules, we investigated their photoluminescence (PL) properties, which display fine emission structure between 500 nm and 590 nm (Figure S3a). A comparison between the absorption and PL excitation spectra (Figure S3c) suggests that the observed emission originates from exfoliated individual NG molecules. Moreover, Figure S3b shows the emission of NGs with the same aromatic core structure, yet, bearing alkyl chains. It exhibits much broader and unstructured emission spectra, with a significant red-shift of the peaks (Figure S3b), which can be attributed to aggregated NGs.[35] Thus, PL studies corroborate that the high shear-mixing approach is highly effective for the exfoliation and dissolution of the NG molecules.

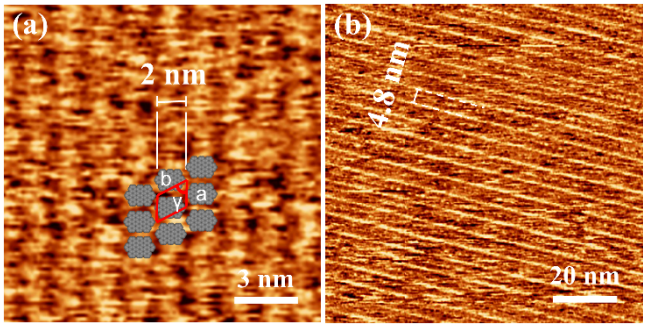

Figure 2. Morphology studies of NG assembly on HOPG surface, in solid film state. STM image of **a)** monolayer and **b)** multilayer NG molecules displaying a crystalline packing characterized the following unit cell: a = 1.3 ± 0.1 nm, b = 2.2 ± 0.1 nm and γ = 70 ± 2°.

In order to study the morphology and structure of NG ultrathin films of monolayer or few-layer thick adsorbates on graphite, the dispersions in NMP are further diluted to a concentration of 1 x 10^{-6} M. After drop-casting 10 µL of the solution onto a freshly cleaved highly oriented pyrolytic graphite (HOPG) surface, the samples are immediately vacuum annealed at 420K overnight, to fully remove the solvent. Scanning Tunneling Microscopy (STM) measurements were performed on dry films at room temperature to gain insight into the molecular structure of NGs after high-shear exfoliation and their self-assembled architectures on HOPG. STM represents an ideal analytical tool to visualize the assembly behavior of large molecules adsorbed on a surface with sub-nanometer spatial resolution. The STM imaging of a monolayer NG film in **Figure 2**a (the 2D-FFT spectrum shown in Figure S5c) confirms the intact molecular structure of the molecules when subjected to our high shear-mixing protocols and subsequent film-formation process, indicating the non-invasive nature of such an exfoliation method, as also confirmed unambiguously by matrix-assisted laser desorption/ionization (MALDI) measurement before and after shear mixing (Figure S4). As a result of resonant tunneling between the Fermi level of the HOPG and the frontier orbital of the adsorbate, the bright areas in the STM height image can be ascribed to the aromatic NG molecules. Due to the planar conformation, the chosen molecules are preferentially packed in a "face-on" fashion onto the basal plane of the HOPG surface. Moreover, the STM images of randomly chosen areas of the multilayer NG film (Figure 2b) exhibit a typical highly ordered long-range crystalline 2D supramolecular packing, stabilized by van der Waals interactions between the molecules and the underlying HOPG surface. Such long-range order is also confirmed on a larger scale by atomic force microscopy (AFM) studies shown in Figure S5a, b.

To explore the optoelectronic properties of the graphene-NG VDWHs, we integrated them as a channel material into photodetectors based on field-effect transistors (FETs). **Figure 3**a portrays the photodetector device geometry (optical microscope

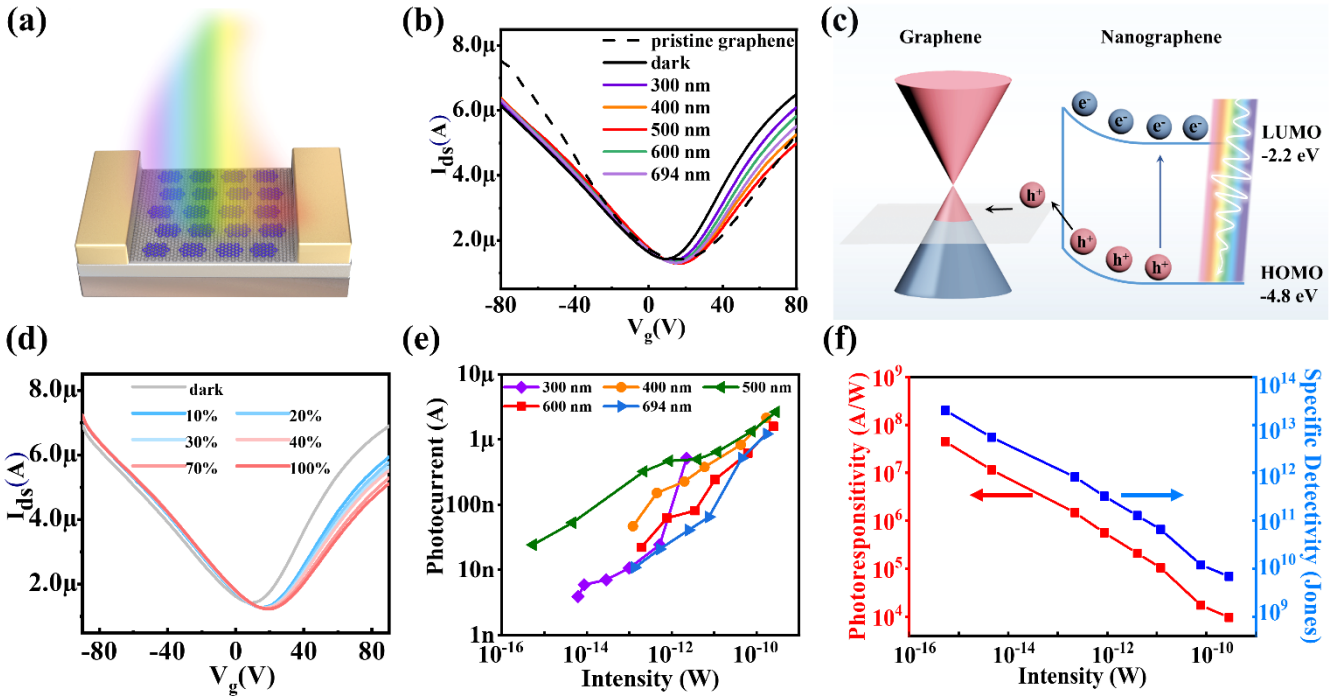

Figure 3. Photodetector based on graphene-NG VDWHs. **a)** Schematic illustration of the photodetector with a FET configuration comprising graphene-NG VDWHs in the device channel. **b)** Transfer characteristics of the FET based on pristine graphene and graphene-NG VDWHs, under dark and different wavelength illumination conditions, V_{ds}=0.01V. **c)** Energy diagram of the graphene-NG VDWHs. Under illumination, photogenerated holes transfer from NG to graphene, while the photogenerated electrons remain in the NG layer. **d)** Transfer characteristics of the FET based on graphene-NG VDWHs, in the dark and different optical illumination powers at 500 nm wavelength, V_{ds}=0.01V. **e)** Photocurrent change upon different optical illumination powers and wavelengths. **f)** Photoresponsivity and specific detectivity change upon different optical illumination powers at 500 nm wavelength.

image shown in Figure S6a). Figure 3b shows the transfer characteristics of the photodetector based on monolayer graphene before and after NG deposition, in the dark and under different illumination wavelengths (from 300 nm to 694 nm), with source-drain voltage V_{ds} kept at 0.01V. The pristine graphene device displays a typical ambipolar behavior with an electron mobility of 1470 cm^2/Vs and a hole mobility of 1700 cm^2/Vs. Following the deposition of NG layer, the V_D corresponding to the Dirac point shifted from 18 V to 6 V, accompanied by an increase of electron mobility to 1540 cm^2/Vs and a decrease of hole mobility to 1320 cm^2/Vs, indicating an n-type doping effect. These phenomena imply that holes migrate from graphene to the NG layer to reach the static charge equilibrium, forming a built-in electric field pointing from the NG layer to graphene at the graphene-NG interface. Under illumination conditions, the Dirac point moves slightly towards positive voltage values and the photocurrent shows a bidirectional behavior with a strong gate-dependence. This suggests a photogating effect in graphene-NG VDWHs and can be rationalized as follows: under light illumination, NG acts as the light-absorbing material generating electron-hole pairs, which are then separated at the interface following hole injection from NG to graphene. The remaining electrons in the NG layer establish a local electric field to gate graphene (Figure 3c), leading to a Fermi-level downshift in graphene and thus a high photoconductive gain. For $V_g < V_D$, where holes are the dominant charge carriers in graphene, the injection of photogenerated holes from NG to graphene enhances the hole density in graphene, thus contributing to a positive photocurrent (Figure S6b). On the contrary, for $V_g > V_D$, where electrons are the major charge carriers in graphene, transfer of photogenerated holes from NG to graphene shifts the E_F of graphene towards the Dirac point, therefore leading to a negative photocurrent. Additionally, it is clear that the photocurrent is higher in the positive gate voltage region because of the work function alignment between the graphene and NG layers. Higher gate voltages increase the Fermi level of graphene thus facilitating the hole transfer to graphene, therefore, in the following we focus on the photocurrent at V_g = 80 V. To demonstrate the importance of the NG within the VDWHs, a control experiment is performed using the pristine graphene photodetector under the same illumination conditions, which shows no significant photoresponse owing to the intrinsically low absorption coefficient of graphene (Figure S7). Further increasing the NG layer thickness results in minor decrease of the photoresponsivity (Figure S5d-f and S8).

Figure 3d depicts the transfer characteristics of the photodetector in the dark and under 500 nm light illumination with different illumination intensities. It reveals a gradual enhancement in the photocurrent upon increasing the illumination intensities from 10% to 100%. Figure 3e portrays the photocurrent of the device under varied illumination wavelengths versus the illumination intensity, suggesting a wide linear dynamic range for most of the illumination conditions, which is one of the key figures of merit for photodetectors. According to the transfer curves in Figure 3b, we estimate the corresponding photoresponsivity as a function of the incident illumination wavelengths as given in Figure S9. The obtained results agree with

the absorption curve of NG molecules, and the device achieves maximum photoresponsivities at 400 nm and 500 nm.

Figure 3f displays the photoresponsivity and specific detectivity of the photodetector at 500 nm over a wide range of illumination intensities. Both of them follow a decrease as the power intensity increases, which is a common phenomenon for such sensitivity tests.[19, 23] At the lowest illumination intensity employed in this study, the device achieves the highest photoresponsivity of 4.5×10^7 A/W, corresponding to a photoconductive gain of 1.1×10^8 and a specific detectivity of 4.6×10^{13} Jones, being competitive with the highest values obtained for graphene-based photodetectors.[15, 19, 23-24] Noteworthily, the photoresponsivity of the devices has not reached saturation at the lowest intensity that can be achieved by our setup, suggesting potentially even higher responsivity at even lower illumination intensity. Moreover, Figure S10 exhibits the temporal photoresponse of a graphene-NG photodetector device under dark and 500 nm illumination conditions during 1000 cycles at $V_g = 80$ V. The photoresponse shows no apparent fatigue during our measured 1000 cycles, proving an excellent endurance and robustness of such devices.

To elucidate the mechanism underlying the observed high photoresponsivity in graphene-NG VDWHs photodetectors, we use optical-pump THz-probe (OPTP) spectroscopy to investigate the ultrafast interfacial charge transfer following optical excitations. For this study, a monolayer of NGs is deposited on CVD-grown graphene supported by SiO_2. The static electronic properties of the graphene with and without NG layers are characterized using Raman and THz time-domain spectroscopy (see Figure S11 and related discussion). These methods give consistent results and show that the graphene prepared for the THz study is initially n-doped, and NG deposition shifts the Fermi level of graphene down from ~260 to ~220 meV. We note a significant difference between graphene used in the devices (produced by exfoliation) and THz studies (made by CVD) in terms of initial and final chemical potential in the graphene sensitized by NGs. Such a difference in chemical potential does not play a role in the direction of charge transfer, as illustrated by device measurements.

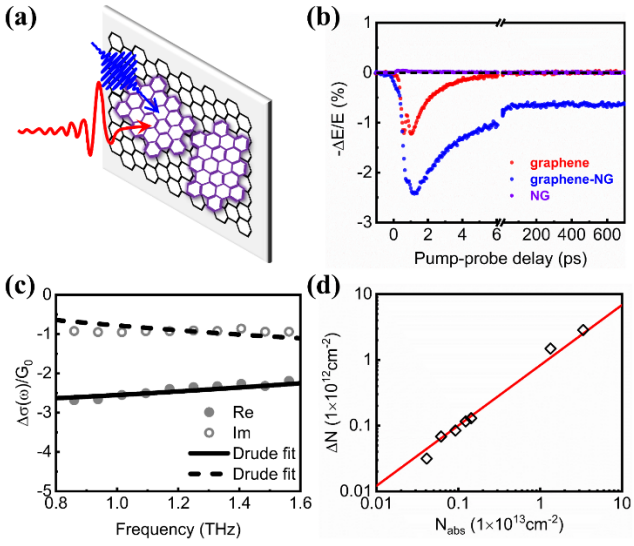

Figure 4. Characterization of charge transfer processes in graphene-NG VDWHs. a) Scheme for optical-pump THz-probe spectroscopy; b) THz photoconductivity dynamics for graphene (red), graphene-NG VDWHs (blue), and NG (purple) following 400 nm excitation (2.8 μJ/cm^2). The measurements are performed in dry N_2 environment. c) Frequency-resolved complex THz photoconductivity for graphene-NG VDWHs at a pump-probe delay of ~100 ps following 400 nm excitation (with a fluence of 16.6 μJ/cm^{-2}). The solid and dashed lines represent the real and imaginary components of the conductivity following the two-parameter Drude model description. d) Quantification of the photoinduced charge transfer efficiency at graphene-NG interfaces.

In the OPTP measurements, the sample is first photoexcited by a short femtosecond laser pulse of 400 nm, and the photoconductivity is then probed by a THz pulse as a function of pump-probe delay, as depicted in **Figure 4**a (see details in SI). For bare graphene, in line with previous OPTP studies,[36-39] photoexcitation of doped graphene leads to a transient reduction in conductivity (i.e., a negative photoconductivity) with a short, ~ 1 ps lifetime (Figure 4b, red dots). The origin of such an effect can be understood as follows: following optical excitation, strong electron-electron scattering leads to the generation of thermalized hot carriers in graphene.[40] These hot carriers exhibit a reduced conductivity in comparison with the cold ones, resulting in negative photoconductivity.[41] As for graphene-NG VDWHs (Figure 4b, blue dots), we find that coating graphene with NG layers slows down the hot carrier cooling (decay dynamics in the first 10 ps) in graphene (See Figure S12 and detailed discussions in SI), to some extent. Furthermore, we observed a remarkably long lifetime beyond 1 ns (limited by our delay line). As a control measurement, we found no photoconductivity for pure NG thin films following the same pump condition (Figure 4b, purple dots). We attribute the long-lived negative photoconductivity observed in the VDWHs to a photoinduced charge transfer (CT) process across the graphene-NG interfaces. Under such a scenario, the photogenerated holes in NG can rapidly transfer to graphene following photoexcitation, resulting in a Fermi-energy downshift in the initially n-doped graphene for over 1 ns before interfacial recombination occurs. The direction and type of the interfacial CT are fully consistent with the device measurements. The long-lived charge separation at the graphene-NG interface allows a high photoconductive gain and partially rationalizes the observed high responsivity in the devices.

Along with the ultralong charge separation, another critical factor determining the device efficiency lies in the charge transfer efficiency following optical excitations. To quantify this, we measured the frequency-resolved THz photoconductivity $\Delta\sigma(\omega)$ (see the description for the method in SI) at a pump-probe delay of 100 ps (where the intrinsic photoresponse of bare graphene is expected to be null). As shown in Figure 4c, we found that $\Delta\sigma(\omega)$ can be described well by the Drude model (see details in SI). Based on this description, we can infer the density and momentum scattering time of the charge carriers following CT. By knowing the initial charge carrier density before photoexcitation (see the characterization for static electronic properties of graphene-NG in Figure S11 and related discussion), one can extract the total density of the transferred holes (ΔN) under different pump fluences, as shown in Figure 4d (See Figure S13 for original dynamics data). This analysis reveals that, in the used fluence range, the amount of transferred holes increases linearly with the absorbed photon density (N_{abs}). To estimate the interfacial CT efficiency η (defined by the ratio between ΔN and photogenerated charge carrier density N_{eh} in NG), we assumed that each absorbed photon creates an electron-hole pair in NG,

i.e., $N_{abs} = N_{eh}$. Under such an assumption, we can estimate a lower bound for the NG-to-graphene hole transfer efficiency η to be ~ 9% (i.e., $\eta > 9\%$). Such a high CT efficiency indicates the enhanced electronic coupling between the NG and graphene layers thanks to the strong interfacial π-π interactions, and rationalizes the superior photodetection performance (together with the ultralong charge separation).

Conclusion

In conclusion, we have demonstrated an efficient high-shear mixing approach to exfoliate the NG aggregates into monodisperse species. Such a protocol can be easily scaled up to produce high-quality solution-processable, low toxicity, and semiconducting NGs for optoelectronics. STM and AFM studies revealed that the NG molecules self-assemble on a HOPG surface, forming highly ordered and tightly packed crystalline films with molecules oriented parallel to the basal plane of the substrate. Thus, the unique physisorption arrangement of NG molecules onto graphene gives rise to the formation of a well-defined superlattice consisting of the graphene-NG VDWHs, with strong interlayer coupling through π-π interactions. The fabricated photodetector based on such VDWHs exhibits an ultrahigh responsivity of 4.5×10^7 A/W and a specific detectivity of 4.6×10^{13} Jones, being competitive with the highest values obtained for graphene-based photodetectors. The excellent device performance can be attributed to the efficient photoinduced hole transfer from NG to graphene and the ultralong charge separation at graphene-NG interfaces, as observed by ultrafast terahertz spectroscopy. Our results demonstrate the great potential of such graphene-NG VDWHs as prototype active components for high-performance, low toxicity optoelectronics. Future efforts in precisely tuning the size and edge structures of NGs may lead to even better synergistic effects of the graphene-NG VDWHs, which could further improve the responsivity and add multicolor detection to the development of flexible photodetectors.

ASSOCIATED CONTENT

Supporting Information

Experimental methods, used equations, UV-Vis, PL, MALDI-TOF, AFM, and THz measurements. This material is available free of charge via the Internet at http://pubs.acs.org."

AUTHOR INFORMATION

Corresponding Author

*samori@unistra.fr

*wanghai@mpip-mainz.mpg.de

Author Contributions

⊥These authors contributed equally to this work. All authors have given approval to the final version of the manuscript.

Notes

The authors declare no competing financial interests.

ACKNOWLEDGMENT

The authors sincerely acknowledge funding from the European Commission through the ERC projects SUPRA2DMAT (GA-833707), the Graphene Flagship Core 3 project (GA-881603), the Agence Nationale de la Recherche through the Labex project CSC (ANR-10-LABX-0026 CSC) within the Investissement d'Avenir program (ANR-10-120 IDEX-0002-02), the International Center for Frontier Research in Chemistry (icFRC), the Institut Universitaire de France (IUF), the Max Planck Society, as well as the German Research Foundation (DFG-Projektnummer 182087777 -SFB 951). H.Q., S.F., and X.Y. acknowledge fellowship support from Chinese Scholarship Council (CSC). The financial support from the Slovenian Research Agency (research core funding No. P1-0055), the ANR-DFG NLE Grant GRANAO by DFG 431450789 and ANR-19-CE09- 0031-01 are also acknowledged.

REFERENCES

1. Du, J.; Pei, S.; Ma, L.; Cheng, H.-M., 25th Anniversary Article: Carbon Nanotube- and Graphene-Based Transparent Conductive Films for Optoelectronic Devices. *Adv. Mater.* **2014,** *26*, 1958-1991.

2. Bonaccorso, F.; Sun, Z.; Hasan, T.; Ferrari, A. C., Graphene Photonics and Optoelectronics. *Nat. Photon.* **2010,** *4*, 611-622.

3. Weiss, N. O.; Zhou, H.; Liao, L.; Liu, Y.; Jiang, S.; Huang, Y.; Duan, X., Graphene: An Emerging Electronic Material. *Adv. Mater.* **2012,** *24*, 5782-5825.

4. Mak, K. F.; Ju, L.; Wang, F.; Heinz, T. F., Optical Spectroscopy of Graphene: From the Far Infrared to the Ultraviolet. *Solid State Commun.* **2012,** *152*, 1341-1349.

5. Nair, R. R.; Blake, P.; Grigorenko, A. N.; Novoselov, K. S.; Booth, T. J.; Stauber, T.; Peres, N. M. R.; Geim, A. K., Fine Structure Constant Defines Visual Transparency of Graphene. *Science* **2008,** *320*, 1308-1308.

6. Liu, C.-H.; Chang, Y.-C.; Norris, T. B.; Zhong, Z., Graphene Photodetectors with Ultra-Broadband and High Responsivity at Room Temperature. *Nat. Nanotechnol.* **2014,** *9*, 273-278.

7. Mueller, T.; Xia, F. N. A.; Avouris, P., Graphene Photodetectors for High-Speed Optical Communications. *Nat. Photon.* **2010,** *4*, 297-301.

8. Xia, F. N.; Mueller, T.; Lin, Y. M.; Valdes-Garcia, A.; Avouris, P., Ultrafast Graphene Photodetector. *Nat. Nanotechnol.* **2009,** *4*, 839-843.

9. Freitag, M.; Low, T.; Xia, F. N.; Avouris, P., Photoconductivity of Biased Graphene. *Nat. Photon.* **2013,** *7*, 53-59.

10. Graham, M. W.; Shi, S.-F.; Ralph, D. C.; Park, J.; McEuen, P. L., Photocurrent Measurements of Supercollision Cooling in Graphene. *Nat. Phys.* **2013,** *9*, 103-108.

11. Brida, D.; Tomadin, A.; Manzoni, C.; Kim, Y. J.; Lombardo, A.; Milana, S.; Nair, R. R.; Novoselov, K. S.; Ferrari, A. C.; Cerullo, G.; Polini, M., Ultrafast Collinear Scattering and Carrier Multiplication in Graphene. *Nat. Commun.* **2013,** *4*, 1987.

12. Gan, X. T.; Shiue, R. J.; Gao, Y. D.; Meric, I.; Heinz, T. F.; Shepard, K.; Hone, J.; Assefa, S.; Englund, D., Chip-Integrated Ultrafast Graphene Photodetector with High Responsivity. *Nat. Photon.* **2013,** *7*, 883-887.

13. Pospischil, A.; Humer, M.; Furchi, M. M.; Bachmann, D.; Guider, R.; Fromherz, T.; Mueller, T., Cmos-Compatible

Graphene Photodetector Covering All Optical Communication Bands. *Nat. Photon.* **2013,** *7*, 892-896.

14. Zhang, Y. Z.; Liu, T.; Meng, B.; Li, X. H.; Liang, G. Z.; Hu, X. N.; Wang, Q. J., Broadband High Photoresponse from Pure Monolayer Graphene Photodetector. *Nat. Commun.* **2013,** *4*, 1811

15. Koppens, F. H. L.; Mueller, T.; Avouris, P.; Ferrari, A. C.; Vitiello, M. S.; Polini, M., Photodetectors Based on Graphene, Other Two-Dimensional Materials and Hybrid Systems. *Nat. Nanotechnol.* **2014,** *9*, 780-793.

16. Liu, J.; Liang, Q.; Zhao, R.; Lei, S.; Hu, W., Application of Organic–Graphene Hybrids in High Performance Photodetectors. *Mater. Chem. Front.* **2020,** *4*, 354-368.

17. Fang, H.; Hu, W., Photogating in Low Dimensional Photodetectors. *Adv. Sci.* **2017,** *4*, 1700323.

18. Jariwala, D.; Marks, T. J.; Hersam, M. C., Mixed-Dimensional Van Der Waals Heterostructures. *Nat. Mater.* **2017,** *16*, 170-181.

19. Konstantatos, G.; Badioli, M.; Gaudreau, L.; Osmond, J.; Bernechea, M.; de Arquer, F. P. G.; Gatti, F.; Koppens, F. H. L., Hybrid Graphene-Quantum Dot Phototransistors with Ultrahigh Gain. *Nat. Nanotechnol.* **2012,** *7*, 363-368.

20. Ni, Z.; Ma, L.; Du, S.; Xu, Y.; Yuan, M.; Fang, H.; Wang, Z.; Xu, M.; Li, D.; Yang, J.; Hu, W.; Pi, X.; Yang, D., Plasmonic Silicon Quantum Dots Enabled High-Sensitivity Ultrabroadband Photodetection of Graphene-Based Hybrid Phototransistors. *ACS Nano* **2017,** *11*, 9854-9862.

21. Aldakov, D.; Reiss, P., Safer-by-Design Fluorescent Nanocrystals: Metal Halide Perovskites Vs Semiconductor Quantum Dots. *J. Phys. Chem. C* **2019,** *123*, 12527-12541.

22. Wang, Q. H.; Kalantar-Zadeh, K.; Kis, A.; Coleman, J. N.; Strano, M. S., Electronics and Optoelectronics of Two-Dimensional Transition Metal Dichalcogenides. *Nat. Nanotechnol.* **2012,** *7*, 699.

23. Roy, K.; Padmanabhan, M.; Goswami, S.; Sai, T. P.; Ramalingam, G.; Raghavan, S.; Ghosh, A., Graphene-Mos2 Hybrid Structures for Multifunctional Photoresponsive Memory Devices. *Nat. Nanotechnol.* **2013,** *8*, 826-830.

24. Zhang, W.; Chuu, C.-P.; Huang, J.-K.; Chen, C.-H.; Tsai, M.-L.; Chang, Y.-H.; Liang, C.-T.; Chen, Y.-Z.; Chueh, Y.-L.; He, J.-H.; Chou, M.-Y.; Li, L.-J., Ultrahigh-Gain Photodetectors Based on Atomically Thin Graphene-Mos2 Heterostructures. *Sci. Rep.* **2014,** *4*, 3826.

25. Wetzelaer, G.-J. A. H.; Kuik, M.; Blom, P. W. M., Identifying the Nature of Charge Recombination in Organic Solar Cells from Charge-Transfer State Electroluminescence. *Adv. Energy Mater.* **2012,** *2*, 1232-1237.

26. Stolterfoht, M.; Armin, A.; Shoaee, S.; Kassal, I.; Burn, P.; Meredith, P., Slower Carriers Limit Charge Generation in Organic Semiconductor Light-Harvesting Systems. *Nat. Commun.* **2016,** *7*, 11944.

27. Bonal, V.; Muñoz-Mármol, R.; Gordillo Gámez, F.; Morales-Vidal, M.; Villalvilla, J. M.; Boj, P. G.; Quintana, J. A.; Gu, Y.; Wu, J.; Casado, J.; Díaz-García, M. A., Solution-Processed Nanographene Distributed Feedback Lasers. *Nat. Commun.* **2019,** *10*, 3327.

28. Kastler, M.; Pisula, W.; Wasserfallen, D.; Pakula, T.; Müllen, K., Influence of Alkyl Substituents on the Solution- and Surface-Organization of Hexa-Peri-Hexabenzocoronenes. *J. Am. Chem. Soc.* **2005,** *127*, 4286-4296.

29. Wasserfallen, D.; Kastler, M.; Pisula, W.; Hofer, W. A.; Fogel, Y.; Wang, Z.; Müllen, K., Suppressing Aggregation in a Large Polycyclic Aromatic Hydrocarbon. *J. Am. Chem. Soc.* **2006,** *128*, 1334-1339.

30. Paternò, G. M.; Nicoli, L.; Chen, Q.; Müllen, K.; Narita, A.; Lanzani, G.; Scotognella, F., Modulation of the Nonlinear Optical Properties of Dibenzo[Hi,St]Ovalene by Peripheral Substituents. *J. Phys. Chem. C* **2018,** *122*, 25007-25013.

31. Hughes, J. M.; Hernandez, Y.; Aherne, D.; Doessel, L.; Müllen, K.; Moreton, B.; White, T. W.; Partridge, C.; Costantini, G.; Shmeliov, A.; Shannon, M.; Nicolosi, V.; Coleman, J. N., High Quality Dispersions of Hexabenzocoronene in Organic Solvents. *J. Am. Chem. Soc.* **2012,** *134*, 12168-12179.

32. Paton, K. R.; Varrla, E.; Backes, C.; Smith, R. J.; Khan, U.; O'Neill, A.; Boland, C.; Lotya, M.; Istrate, O. M.; King, P.; Higgins, T.; Barwich, S.; May, P.; Puczkarski, P.; Ahmed, I.; Moebius, M.; Pettersson, H.; Long, E.; Coelho, J.; O'Brien, S. E.*, et al.*, Scalable Production of Large Quantities of Defect-Free Few-Layer Graphene by Shear Exfoliation in Liquids. *Nat. Mater.* **2014,** *13*, 624-630.

33. Iyer, V. S.; Yoshimura, K.; Enkelmann, V.; Epsch, R.; Rabe, J. P.; Müllen, K., A Soluble C60 Graphite Segment. *Angew. Chem. Int. Ed.* **1998,** *37*, 2696-2699.

34. Hernandez, Y.; Nicolosi, V.; Lotya, M.; Blighe, F. M.; Sun, Z.; De, S.; McGovern, I. T.; Holland, B.; Byrne, M.; Gun'Ko, Y. K.; Boland, J. J.; Niraj, P.; Duesberg, G.; Krishnamurthy, S.; Goodhue, R.; Hutchison, J.; Scardaci, V.; Ferrari, A. C.; Coleman, J. N., High-Yield Production of Graphene by Liquid-Phase Exfoliation of Graphite. *Nat. Nanotechnol.* **2008,** *3*, 563-568.

35. Englert, J. M.; Hauke, F.; Feng, X.; Müllen, K.; Hirsch, A., Exfoliation of Hexa-Peri-Hexabenzocoronene in Water. *Chem. Commun.* **2010,** *46*, 9194-9196.

36. Shi, S. F.; Tang, T. T.; Zeng, B.; Ju, L.; Zhou, Q.; Zettl, A.; Wang, F., Controlling Graphene Ultrafast Hot Carrier Response from Metal-Like to Semiconductor-Like by Electrostatic Gating. *Nano Lett.* **2014,** *14*, 1578-1582.

37. Frenzel, A. J.; Lui, C. H.; Shin, Y. C.; Kong, J.; Gedik, N., Semiconducting-to-Metallic Photoconductivity Crossover and Temperature-Dependent Drude Weight in Graphene. *Phys. Rev. Lett.* **2014,** *113*, 056602.

38. Tielrooij, K. J.; Song, J. C. W.; Jensen, S. A.; Centeno, A.; Pesquera, A.; Zurutuza Elorza, A.; Bonn, M.; Levitov, L. S.; Koppens, F. H. L., Photoexcitation Cascade and Multiple Hot-Carrier Generation in Graphene. *Nat. Phys.* **2013,** *9*, 248-252.

39. Jnawali, G.; Rao, Y.; Yan, H.; Heinz, T. F., Observation of a Transient Decrease in Terahertz Conductivity of Single-Layer Graphene Induced by Ultrafast Optical Excitation. *Nano Lett.* **2013,** *13*, 524-530.

40. Gierz, I.; Petersen, J. C.; Mitrano, M.; Cacho, C.; Turcu, I. C. E.; Springate, E.; Stöhr, A.; Köhler, A.; Starke, U.; Cavalleri, A., Snapshots of Non-Equilibrium Dirac Carrier Distributions in Graphene. *Nat. Mater.* **2013,** *12*, 1119-1124.

41. Tomadin, A.; Hornett, S. M.; Wang, H. I.; Alexeev, E. M.; Candini, A.; Coletti, C.; Turchinovich, D.; Kläui, M.; Bonn, M.; Koppens, F. H. L.; Hendry, E.; Polini, M.; Tielrooij, K.-J., The Ultrafast Dynamics and Conductivity of Photoexcited Graphene at Different Fermi Energies. *Sci. Adv.* **2018,** *4*, 5313.